

Communication

# Tripodal Oxazolidine-N-Oxyl Diradical Complexes of Dy<sup>3+</sup> and Eu<sup>3+</sup>

Philippe Rey <sup>1</sup>, Andrea Caneschi <sup>2</sup>, Taisiya S. Sukhikh <sup>1</sup> and Kira E. Vostrikova <sup>1,\*</sup>

<sup>1</sup> Nikolaev Institute of Inorganic Chemistry, Siberian Branch, Russian Academy of Sciences, 630090 Novosibirsk, Russia; philippe.rey@etu.univ-grenoble-alpes.fr (P.R.); sukhikh@niic.nsc.ru (T.S.S.)  
<sup>2</sup> INSTM Research Unit of Firenze, Dipartimento di Ingegneria Industriale-DIEF, Università degli Studi di Firenze, Via di Santa Marta n. 3, 50139 Firenze, Italy; andrea.caneschi@unifi.it

\* Correspondence: vosk@niic.nsc.ru

**Abstract:** Two diradical complexes of the formula [LnRad<sub>2</sub>(CF<sub>3</sub>SO<sub>3</sub>)<sub>3</sub>] c (Ln(III) = Dy, Eu, Rad = 4,4-dimethyl-2,2-bis(pyridin-2-yl)-1,3-oxazolidine-3-oxyl) were obtained in air conditions. These are the first examples of diradical compounds of lanthanides and oxazolidine nitroxide. The complexes were characterized crystallographically and magnetically. Single crystal XRD analysis revealed that their coordination sphere is composed of three monodentate triflates and two tripodal Rad, which coordinate the central atom in a tridentate manner via two N atoms of the pyridine groups and the O atom of a nitroxide group. The LnO<sub>5</sub>N<sub>4</sub> polyhedron represents a spherical capped square antiprism with point symmetry close to C<sub>4v</sub>. The data of static magnetic measurements are compatible with the presence of two paramagnetic ligands in the coordination sphere of the metal.

**Keywords:** complexes; stable organic radical; tripodal ligands; oxazolidine nitroxyl radical; heterospin systems; magnetic properties; molecular magnetism



**Citation:** Rey, P.; Caneschi, A.; Sukhikh, T.S.; Vostrikova, K.E. Tripodal Oxazolidine-N-Oxyl Diradical Complexes of Dy<sup>3+</sup> and Eu<sup>3+</sup>. *Inorganics* **2021**, *9*, 91. <https://doi.org/10.3390/inorganics9120091>

Academic Editors: Leonor Maria and Joaquim Marçalo

Received: 28 November 2021  
Accepted: 18 December 2021  
Published: 20 December 2021

**Publisher's Note:** MDPI stays neutral with regard to jurisdictional claims in published maps and institutional affiliations.



**Copyright:** © 2021 by the authors. Licensee MDPI, Basel, Switzerland. This article is an open access article distributed under the terms and conditions of the Creative Commons Attribution (CC BY) license (<https://creativecommons.org/licenses/by/4.0/>).

## 1. Introduction

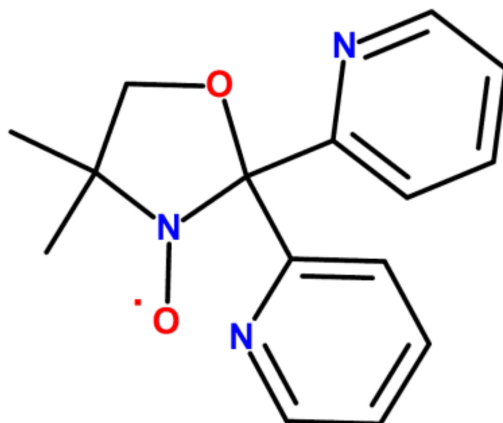
The study of single-molecule magnets (SMMs) is the most intensively developing area of molecular magnetism. SMMs are molecules possessing an energetic barrier to magnetic relaxation that allows them to keep their magnetization orientation after switching off the magnetic field. Moreover, these molecules exhibit bulk magnet-like property-magnetic hysteresis, and their nanosize nature leads to quantum tunnelling of the magnetization (QTM). The discovery of slow magnetic relaxation at the molecular level has generated tremendous interest in SMMs, essentially due to the possibility of their use in molecular spintronics [1–6] and quantum information storage and processing [7–10]. However, in order to realize these applications, much higher spin relaxation barriers (SRBs) must be attained.

Since the SRB height is determined by the square of the total spin of the molecule and its axial anisotropy, it is necessary to increase both of these parameters. It should be emphasized that the latter is very important [11] for the design of high-temperature SMMs. This is why in the last decade, researchers have paid special attention to the synthesis and study of single-ion magnets based on trivalent lanthanides, since they have large magnetic anisotropy due to significant spin–orbit interaction [11–13]. The combination of the used lanthanide nature and ligand field environment has permitted chemists to make SMMs displaying magnetic memory at a temperature up to 80 K [14,15]. Strong axial anisotropy can be enforced by an appropriate design of the crystal field splitting (CFS) [13,16–18], and the provision of large enough energy splitting on the Ln sites is required to reduce the QTM between ground states. For this reason, it is very important to study minor changes in ligand-field strength associated with the coordination polyhedrons of the Ln<sup>III</sup> complexes. However, it is hard to implement systematic control of the coordination geometries and the ligand-field strength of Ln<sup>III</sup> compounds [19].

In addition, the internal 4f electrons are largely shielded by external electrons. It reduces magnetic exchange interaction as it will short cut the anisotropy barrier [20]. Therefore, an exceptionally high SRB will not certainly lead to a high blocking temperature if the exchange coupling is not strong. Moreover, strong exchange coupling can help to switch off QTM within a single spin state manifold [20]. In this case, radical ligands may be considered as being especially suitable for supporting strong spin coupling, and study the influence over the slow relaxation process of the magnetization [20].

Most Ln-SMMs, especially the ones based on Ln with a large value of the total angular momentum [21], exhibit magnetization blocking in a low-symmetry ligand environment often with a coordination number of 6 to 10 [22]. An ideal point group symmetry, such as  $C_{\infty v}$ ,  $D_{4d}$ ,  $S_8$ ,  $D_{5h}$ ,  $D_{6d}$ , and  $D_{\infty h}$ , could efficiently suppress the undesirable QTM process [16,23–26]. Therefore, a current challenge is the choice of ligands, which can lead to the formation of a coordination environment that is optimal for obtaining maximum axial magnetic anisotropy and minimum QTM.

Quite recently, we obtained several nitrate complexes of Ln(III) involving a tripodal nitroxyl radical 4,4-dimethyl-2,2-bis(pyridin-2-yl)-1,3-oxazolidine-3-oxyl (Rad) (Scheme 1) [27]. The obtained value of  $23 \text{ cm}^{-1}$  ( $+JS_1S_2$  formalism) for the antiferromagnetic metal-radical coupling in  $[\text{GdRad}(\text{NO}_3)_3]$  established from the magnetic and EPR data is remarkable for complexes of 4f-elements with nitroxyl radicals. The terbium congener displays frequency-dependent out-of-phase signals in the zero field designating single-molecule magnetic behavior.



**Scheme 1.** Tridentate radical-4,4-dimethyl-2,2-bis(pyridin-2-yl)-1,3-oxazolidine-3-oxyl (Rad).

This work presents the results of the first experiments on obtaining diradical complexes of  $\text{Ln}^{\text{III}}$  and Rad. In contrast to 3d metals, for which a long series of complexes  $[\text{M}^{3d}\text{Rad}_2]^{2+}$  with different anions were obtained [28–35], and two Ni(II) complexes with one radical [33], diradical lanthanide complexes of Rad have not been known until now. Our objective was to demonstrate the principal possibility of preparation of the Ln(III) complexes containing two tripodal nitroxyl radicals (Rad). The compounds  $[\text{LnRad}_2](\text{anion})_3$  with a six-coordinated environment similar to that of the previously obtained Dy compounds [36,37] would be especially promising from the point of view of their magnetic behavior.

## 2. Results and Discussion

### 2.1. Synthetic Aspects and IR Spectra of the Complexes

The reaction of a dichloromethane solution containing the stoichiometric amounts of  $\text{Dy}(\text{CF}_3\text{SO}_3)_3$  and 4,4-dimethyl-2,2-bis(pyridin-2-yl)-1,3-oxazolidine-3-oxyl (Rad) (Scheme 1) at  $40^\circ\text{C}$  afforded the diradical complex  $[\text{DyRad}_2(\text{CF}_3\text{SO}_3)_3]$  (**1**). Saturation of the reaction mixture with diethyl ether vapors led to the crystals  $1 \cdot 0.5\text{CH}_2\text{Cl}_2 \cdot 0.5\text{Et}_2\text{O}$  incorporating a small amount of both solvent molecules, which are losing readily during storage or

manipulations with the compounds. The paramagnetic ligand is stable in air, both in solid form and in non-aqueous solutions, even when heated.

Earlier, the diradical complexes of divalent *3d* metal ions, including trimethylsulfonate as a counterion, were obtained [28]. It should be noted that no hydrolysis of the starting ligand was detected upon Rad complexation for *3d* metal ions with different counterions [28–35]. However, in the case of the lanthanide ions, which are known by their catalytic properties towards organic entities resulting in the breaking of covalent bonds [38,39], additional precautions are needed. In addition, one should pay attention to the humidity and the reaction rate to avoid by-product formation.

The europium analogue, [EuRad<sub>2</sub>(CF<sub>3</sub>SO<sub>3</sub>)<sub>3</sub>] (**2**), was prepared similarly to **1**. However, during saturation of the reaction solution by ether vapors for one night at 4 °C, a small amount of a binuclear compound [Eu<sub>2</sub>(*dpk*)<sub>2</sub>(*hbpm*)<sub>2</sub>(CF<sub>3</sub>SO<sub>3</sub>)<sub>2</sub>] (*dpk* is di(2-pyridyl) ketone and *hbpm* is hydroxybis(2-pyridyl)methanolate) (**3**) formed. The colorless crystals of the complex **3** were separated by filtration, and the mother liquor was left for an additional saturation for few days, giving the orange crystals of solvated **2**·CH<sub>2</sub>Cl<sub>2</sub>. As in the case of its Dy congener, the solvate molecules are readily lost to give unsolvated bulk compound **2**. The formation of **3** is apparently due to a partial catalytic hydrolysis of the radical (Figure S1, see the Supplementary Materials).

The IR spectra (SI, Figure S2) for **1** and **2** are very similar. The frequencies of the groups involved in coordination are shifted towards lower energy compared with those of free ligands. The most intense are the triflate absorption bands, and their positions shifted compared to those of non-coordinated triflate [40], confirming the coordinated character of the anions. Moreover, the greatest shift is experienced by the bands of the SO<sub>3</sub> groups while the shifts of the CF<sub>3</sub> groups are much smaller.

In the coordination chemistry of *d*-elements, triflates are usually used as low-coordinating anions. However, in the case of lanthanide ions with high coordination numbers, neutral polydentate ligands must be sterically hindered enough so that the triflate anions do not fit around the central atom. In the case of the tripodal Rad, its stericity is not sufficient to prevent the entrance of counterions into the inner sphere of the complex.

To solve this problem, attempts were made to synthesize diradical complexes using bulky anions as counterions: iodide and tetraphenylborate. However, upon the addition of acetonitrile solutions of Ln(Ph<sub>4</sub>B)<sub>3</sub> or LnI<sub>3</sub> complexes to a solution of the radical in the same solvent, the yellow color of the reaction mixture gradually changed to red, and upon slow evaporation of the solvent, a red-brown viscous product was formed. Most likely, this is due to the reduction of the radical mediated by [Ph<sub>4</sub>B]<sup>−</sup>, as it was found earlier for the Rad [29,30]. An additional argument in favor of Rad<sup>−</sup> formation when using reducing iodide and PPh<sub>4</sub>B<sup>−</sup> is the interaction of [Sm{N(SiMe<sub>3</sub>)<sub>2</sub>]<sub>2</sub>] with TEMPO ((2,2,6,6-Tetramethylpiperidin-1-yl)oxyl-closely related radical), which led to reddening of the reaction mixture, giving the complex[Sm{N(SiMe<sub>3</sub>)<sub>2</sub>]<sub>2</sub>TEMPO<sup>−</sup>] [41].

## 2.2. Description of the Crystal Structures 1–3

According to the single crystal X-ray analysis, both tripodal Rad coordinate the central atom in a tridentate manner via two N atoms of the pyridine groups and the O atom of the NO moiety (Figure 1) similarly to that in previously reported Zn(II), Cu(II) [28] and Ln(III) [27] complexes with Rad. The coordination sphere is complemented by three monodentate triflates to give DyO<sub>5</sub>N<sub>4</sub> polyhedron. The Continuous Symmetry Measures (CSM) analysis [42] gave the description of the polyhedron as a spherical capped square antiprism (Figure 2) with the point symmetry close to C<sub>4v</sub> (Table S1)<sup>†</sup> as the best fit. The donor atoms of Rad and two triflates compose faces of the antiprism while oxygen of the third triflate arranges above the rectangular face.

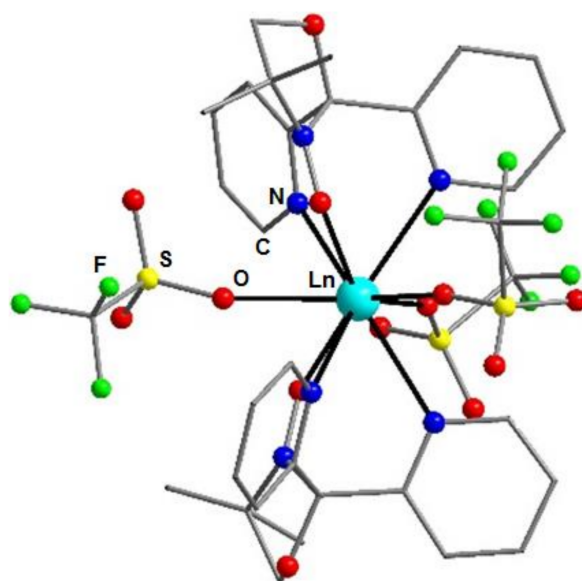


**Figure 1.** Structure of molecules 1 and 2. Hydrogen atoms are not shown.

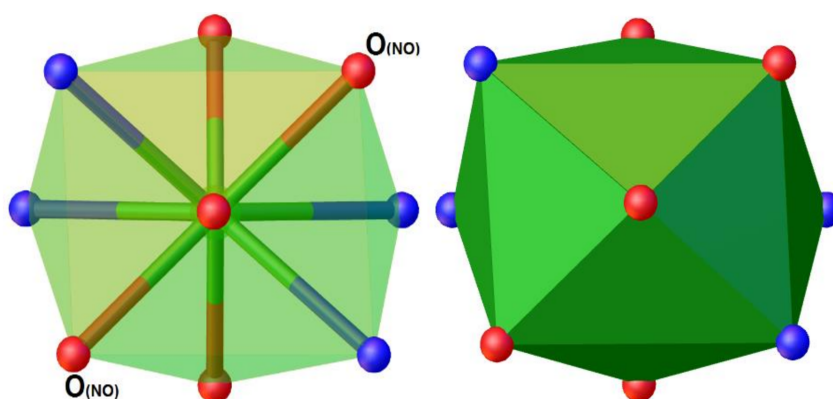


**Figure 2.** The  $\text{LnO}_5\text{N}_4$  polyhedron-spherical capped square antiprism.

The  $[\text{Eu}_2(\text{dpk})_2(\text{hbp})_2(\text{CF}_3\text{SO}_3)_2]$  (**3**) is a binuclear compound in which the two di(2-pyridyl) ketone act as the chelate bidentate ligands, while the two anions of hydroxybis(2-pyridyl)methanolate are tridentate, with olate oxygen being a bridging moiety (Figure 3).

### 2.3. Magnetic Properties

The SQUID magnetometry results on polycrystalline complexes **1** and **2** are shown in Figure 4. The  $\chi_m T$  value at 300 K of  $14.735 \text{ emu K mol}^{-1}$  for **1** is slightly smaller than the theoretical value of  $14.92 \text{ emu K mol}^{-1}$  at the non-interacting limit from two radicals ( $S = 1/2$ ,  $g = 2.0023$ ,  $0.375 \text{ emu K mol}^{-1}$ ) and one  $\text{Dy}^{\text{III}}$  ion ( $4f^9$ ,  $S = 5/2$ ,  $L = 5$ ,  $J = 15/2$ ,  $g_J = 4/3$ ,  ${}^6\text{H}_{15/2}$ ,  $14.17 \text{ emu K mol}^{-1}$ ). This value is, however, in good agreement with the those of  $14.365 \text{ emu K mol}^{-1}$ , previously obtained for the monoradical complex  $[\text{DyRad}(\text{NO}_3)_3]$  [27] taking into account the fact that the experimental values for dysprosium in a related coordination environment are somewhat lower than those for a free ion:  $13.92\text{--}14.00$  [43,44]. On cooling, the  $\chi_m T$  value remains virtually unchanged up to 90 K, and then gradually decreases down to  $10 \text{ emu K mol}^{-1}$  at 20 K and finely drops to  $4.803 \text{ emu K mol}^{-1}$  at 2 K. The last value is considerably lower than that for the monoradical analogue ( $6.50 \text{ emu K mol}^{-1}$ ). Since substantial intermolecular exchange interactions in **1** can be excluded, the origin of such behavior could be attributed to the radical-radical coupling, which can reach high values ( $J_{\text{TEMPO1-TEMPO2}}/k_B = -24.9 \text{ K}$ ) in  $[\text{Y}(\text{hfac})_3(\text{TEMPO})_2]$  [45].

Moreover, the metal-to-radical coupling in the  $[\text{Gd}(\text{hfac})_3(\text{TEMPO})_2]$  has been reported to be either positive or negative for the different radicals of the same molecule ( $J_{\text{Gd-TEMPO}}/k_B = -6.45$  and  $+4.0$  K, complicating the picture. Therefore, for the highly anisotropic Dy, it is difficult to obtain more information also due to the high mixing of the  $|J, m_J\rangle$  levels favored by the relatively low-symmetry ligand field. In order to elucidate the nature of exchange interactions in **1**, experimental magnetic measurements and theoretical calculations for yttrium and gadolinium diradical complexes are in progress.

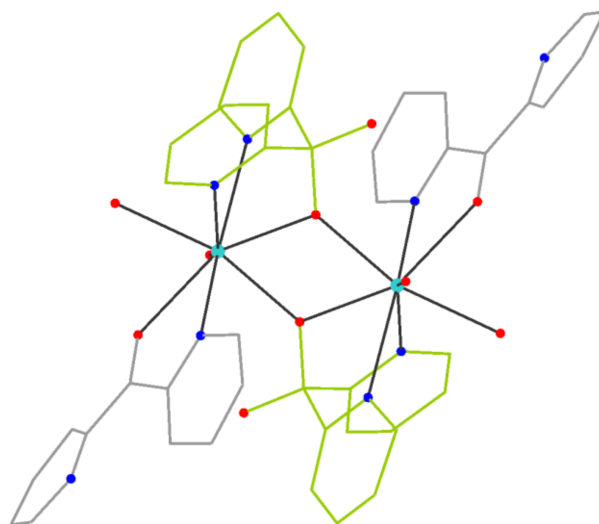


**Figure 3.** Molecular structure of the complex **3**. Hydroxybis(2-pyridyl)methanolate is shown green. Non-coordinated atoms of the triflates and hydrogens are not shown.

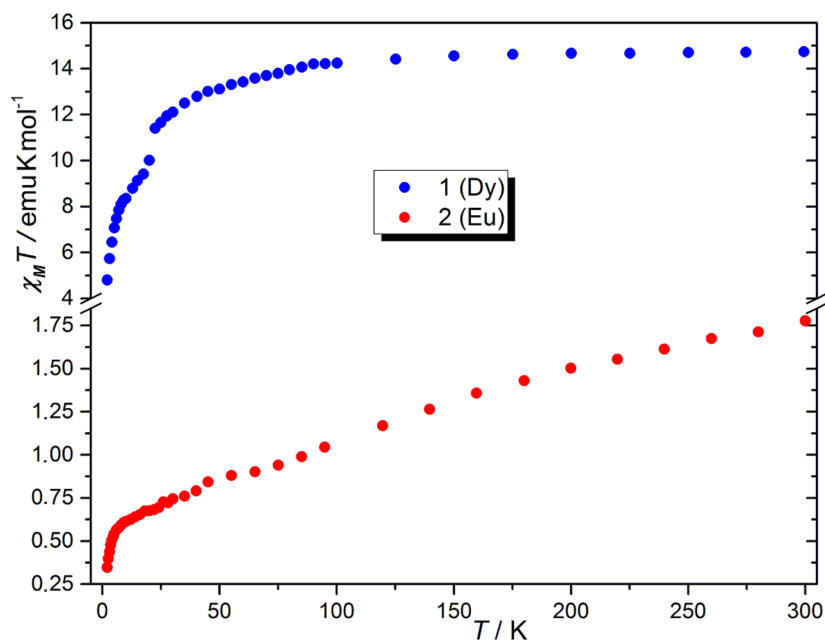


**Figure 4.** Temperature dependencies of  $\chi_M T$  products for **1** and **2**.

The temperature dependence of  $\chi_M T$  for europium complexes is determined by the thermal population of the  ${}^7F_1$  level nearest to the ground nonmagnetic level  ${}^7F_0$ . The excited  ${}^7F_1$  state, closely located to the ground one, is populated in part already at room temperature. At 300 K,  $\chi_M T$  for europium(III) complexes with diamagnetic organic ligands can vary in the range of 1.032–1.386  $\text{emu K mol}^{-1}$  depending on the ligand field parameters [46]. Consequently, for the complex **2**, the room temperature  $\chi_M T$  value of

1.778 emu K mol<sup>-1</sup> is reasonable for the two uncoupled radicals and one Eu<sup>3+</sup> ion but lower than the value of 1.93 emu K mol<sup>-1</sup> found for the bis-nitronyl nitroxide (NN) complex [Eu(NN)<sub>2</sub>(NO<sub>3</sub>)<sub>3</sub>] with a different coordination number and mode (N<sub>10</sub> instead of N<sub>4</sub>O<sub>5</sub>) [47]. As the temperature is lowered, the  $\chi_m T$  decreases gradually, and, starting from 9 K, drops to 0.348 emu K mol<sup>-1</sup>, which is somewhat higher than that for [Eu(NN)<sub>2</sub>(NO<sub>3</sub>)<sub>3</sub>] compound (0.24 emu K mol<sup>-1</sup>). The magnetization plots (*M* vs. *B*) for **1** and **2** recorded up to 50,000 Oe at the temperatures of 2, 5, and 10 K are reported in Figure S3. No ac signal was observed in either sample in the measurable interval of frequencies (0.1–10,000 Hz).

### 3. Experimental Section

#### 3.1. Materials and Physical Measurements

Ln(CF<sub>3</sub>SO)<sub>3</sub> salts (Thermo Fisher GmbH, Kandel, Germany) were purchased from Alfa Aesar. Dichloromethane (EKOS-1, Moscow, Russia) was distilled prior to use. 2,2'-Dipyridyl ketone (99%) (Sigma-Aldrich, Saint Louis, MO, USA) was used as received. The 4,4-dimethyl-2,2-bis(pyridin-2-yl)-1,3-oxazolidine N-oxyl radical was synthesized according to a known procedure [28]. The complexes were synthesized under aerobic conditions. Elemental (C, H, N, S) analyses were carried out by standard methods with a Euro-Vector 3000 analyser (Eurovector, Redavalle, Italy). Powder XRD was carried out using a Shimadzu XRD-7000S diffractometer (Shimadzu, Kyoto, Japan) (CuK $\alpha$  radiation, Ni filter, 2 $\theta$  angle range from 5° to 30°) using a Dectris MYTHEN2 R 1K detector ( $\lambda$  = 1.54178 Å, Kyoto, Japan). Simulated patterns from the X-ray crystal structure were obtained with Diamond 3.0 (Crystal Impact GbR: Bonn, Germany) from the crystal structures of **1**·0.5CH<sub>2</sub>Cl<sub>2</sub>·0.5Et<sub>2</sub>O and **2**·CH<sub>2</sub>Cl<sub>2</sub>. Fourier transform infrared (FTIR) spectra were measured in KBr pellets with a Perkin–Elmer System 2000 FTIR spectrometer (Perkin Elmer, Waltham, MA, USA) in the 4000–400 cm<sup>-1</sup> range. The DC and AC magnetic properties of the compounds were determined by measuring polycrystalline samples pressed in Teflon pellet to avoid preferential orientation of the crystallites, using a QD MPMS SQUID magnetometer (Quantum Design GmbH, Darmstadt, Germany) in the temperature range 1.9–300 K with an applied field up to 5.5 T in the frequency range 1–10,000 Hz (for ac characterization). The intrinsic diamagnetic contributions of the samples were estimated using Pascal's Constants [48].

#### 3.2. Synthesis of the Complexes

**[DyRad<sub>2</sub>(CF<sub>3</sub>SO<sub>3</sub>)<sub>3</sub>]** A solution of Dy(CF<sub>3</sub>SO<sub>3</sub>)<sub>3</sub>·(61 mg, 0.100 mmol) in CH<sub>2</sub>Cl<sub>2</sub> (2 mL) was added dropwise to a stirred solution of Rad (60 mg, 0.222 mmol) in CH<sub>2</sub>Cl<sub>2</sub> (2 mL). Upon agitation at 40 °C, the reaction mixture gradually turned lemon yellow. The crystalline product **1**·0.5CH<sub>2</sub>Cl<sub>2</sub>·0.5Et<sub>2</sub>O was obtained after the evaporation 50% of the solvent followed by a slow saturation with ether vapors at 4 °C. Drying of the compound resulted in unsolvated **1**. Yield: 49 mg (43%). Anal. calcd. (%) for C<sub>33</sub>H<sub>32</sub>DyF<sub>9</sub>N<sub>6</sub>O<sub>13</sub>S<sub>3</sub>: C, 34.5; H, 2.8; N, 7.3; S, 8.4. Found: C, 34.7; H, 2.9; N, 7.0; S, 8.1. IR (KBr):  $\nu$  (cm<sup>-1</sup>) 2985(w) 2940(w) 2895(w) 1603 (m) 1576(w) 1487(sh) 1472(m) 1441(m) 1387(w) 1373(w) 1319(s) 1283(sh) 1251(sh) 1236(s) 1211(s) 1177(sh) 1167(s) 1101(w) 1076(w) 1063(w) 1030(s) 1018(sh) 1001(m) 976(w) 958(w) 941(w) 930(w) 773(w) 762(sh) 750(sh) 708(w) 677(w) 662(w) 637(m) 582(w) 515(w) 430(w) 420(w).

**[EuRad<sub>2</sub>(CF<sub>3</sub>SO<sub>3</sub>)<sub>3</sub>]·CH<sub>2</sub>Cl<sub>2</sub> (2)** and **[Eu<sub>2</sub>(dpk)<sub>2</sub>(dpmo)<sub>2</sub>(CF<sub>3</sub>SO<sub>3</sub>)<sub>2</sub>] (3)** To a solution of Eu(CF<sub>3</sub>SO<sub>3</sub>)<sub>3</sub>·(62 mg, 0.103 mmol) in CH<sub>2</sub>Cl<sub>2</sub> (2 mL) was added dropwise to a stirred solution of Rad (60 mg, 0.222 mmol) in CH<sub>2</sub>Cl<sub>2</sub> (1.5 mL). The reaction mixture was heated at 40 °C for 15 min. Then, it was filtered and set to saturate with ether vapors at 4 °C. After two days, a small amount of thin colorless crystals of (3) formed. The crystals were isolated by filtration. Further saturation of the reaction mixture with ether vapors led to the formation of one big orange-yellow grown-together polycrystalline block of **2**·CH<sub>2</sub>Cl<sub>2</sub>, which was separated from the mother liquor, rinsed by a small amount of cold dichloromethane, and air-dried to give unsolvated **2**. Yield: 48%. C<sub>33</sub>H<sub>32</sub>EuF<sub>9</sub>N<sub>6</sub>O<sub>13</sub>S<sub>3</sub>

(1139.79 g/mol): Anal. calcd.: C, 34.8, H, 2.8, N, 7.4; S, 8.4; found: C, 34.6, H, 2.6, N, 7.2; S, 7.82. IR (KBr): very similar to those of 1 (see Supplementary Materials).

[Eu<sub>2</sub>(dpk)<sub>2</sub>(hdpmo)<sub>2</sub>(CF<sub>3</sub>SO<sub>3</sub>)<sub>2</sub>] (3) Yield: 5 mg. C<sub>48</sub>H<sub>34</sub>Eu<sub>2</sub>F<sub>12</sub>N<sub>8</sub>O<sub>18</sub>S<sub>4</sub> (1668.98 g/mol).

### 3.3. Single-Crystal X-ray Crystallography Data Collection and Refinement

Single crystals were coated with Nujol and were quickly mounted on MicroLoops (MiTeGen LLC., Ithaca, NY, USA) and immediately cooled in a N<sub>2</sub> cold stream to avoid decomposition. The data collection was performed at 150 K on a Bruker D8 Venture diffractometer (Bruker AXS, Karlsruhe, Germany) with a CMOS PHOTON III detector and I $\mu$ S 3.0 microfocus source (collimating Montel mirrors, MoK $\alpha$  radiation). The crystal structures were solved using the SHELXT [49] and were refined using SHELXL [50] programs with OLEX2 GUI [51]. Atomic displacement parameters for non-hydrogen atoms of 1–2 were refined anisotropically. Hydrogen atoms were placed geometrically. Due to the poor quality of crystals of compound 3, the structure reveals a number of checkcif alerts. N atoms and most C atoms were refined in the isotropic approximation to maintain a reasonable data-to-parameters ratio. Nonetheless, the structure is reported to show the approximate geometry of the complex. CCDC 2121366–2121368 for 1–3 contain the supplementary crystallographic data for this paper, and can be obtained free of charge from the Cambridge Crystallographic Data Centre via <https://www.ccdc.cam.ac.uk/structures/> (accessed on 28 November 2021).

## 4. Conclusions and Perspectives

For the first time, we demonstrated a principal possibility of obtaining diradical complexes 1 and 2 of Ln(III) with a functionalized oxazolidine radical. The latter, being a tridentate ligand, is distinguished by a stereochemical rigidity and a predictable tripodal manner of coordination. Therefore, such a radical is promising for the synthesis of low-coordinate complexes with an axial symmetry required for QTM quenching [31]. The synthesized compounds [LnRad<sub>2</sub>(CF<sub>3</sub>SO<sub>3</sub>)<sub>3</sub>] feature a rather high coordination number, 9, which is due to insufficient steric demanding not only of the tripod, but also of the anionic ligands. To ensure a satisfactory bulkiness of a paramagnetic ligand to prepare complexes [LnL<sub>2</sub>]<sup>3+</sup> with a coordination number of six, it could be sufficient to use a Rad derivative with a methyl group at the sixth position of the pyridine ring. In our opinion, the most suitable counterion could be tetrakis(pentafluorophenyl)borate, which, unlike its unfluorinated analogue [29,30], should not be a reducing agent for the Rad [31].

In the short term, we are faced with the objective of expanding the range of diradical complexes of lanthanides with Rad in order to clarify the nature of the magnetic exchange interactions between paramagnetic centers in {LnRad<sub>2</sub>} systems. For this purpose, it is necessary, first of all, to synthesize and study magnetochemically the isostructural compounds of diamagnetic yttrium(III) and lutetium(III) in order to have an idea of the radical-radical coupling. Analysis of the magnetic behavior of the diradical complex of the isotropic ion Gd<sup>3+</sup> will provide the information on Ln–Rad interactions. It is also interesting to check whether the terbium complex will exhibit slow magnetic relaxation, since for its monoradical congener, it was earlier recorded.

**Supplementary Materials:** The following are available online at <https://www.mdpi.com/article/10.3390/inorganics9120091/s1>, Figure S1: Catalytic hydrolysis transformation of the paramagnetic ligand, Table S1: Geometry analysis of the complexes by SHAPE software, Table S2: Crystal data and structure refinement for compounds 1–3; Figure S2: FTIR spectra of 1 and 2, Figure S3: M/H plots for 1 and 2 at the different temperatures. Figure S4: PXRD patterns for 1 and 2.

**Author Contributions:** Conceptualization, K.E.V.; methodology, K.E.V. and T.S.S.; investigation, P.R. and A.C.; resources, T.S.S.; writing—original draft preparation, P.R. and K.E.V.; writing—review and editing, K.E.V. and T.S.S.; visualization, K.E.V. and T.S.S.; supervision, K.E.V. and T.S.S.; project administration, T.S.S.; funding acquisition, T.S.S. All authors have read and agreed to the published version of the manuscript.

**Funding:** This research was funded by RFBR according to the research project No. 20-33-70172. The XRD and the IR studies were carried out with the support of the Ministry of Science and Higher Education of the Russian Federation (No. 121031700313-8 and No. 121031700321-3).

**Data Availability Statement:** CCDC 2121366–2121368 for 1–3 contain the supplementary crystallographic data for this paper, and can be obtained free of charge from The Cambridge Crystallographic Data Centre via <https://www.ccdc.cam.ac.uk/structures/> (accessed on 28 November 2021).

**Acknowledgments:** Mauro Perfetti is kindly acknowledged for stimulating scientific discussion.

**Conflicts of Interest:** The authors declare no conflict of interest.

## References

1. Bogani, L.; Wernsdorfer, W. Molecular Spintronics Using Single-Molecule Magnets. *Nat. Mater.* **2008**, *7*, 179–186. [[CrossRef](#)] [[PubMed](#)]
2. Liang, W.; Shores, M.P.; Bockrath, M.; Long, J.R.; Park, H. Kondo Resonance in a Single-Molecule Transistor. *Nature* **2002**, *417*, 725–729. [[CrossRef](#)]
3. Urdampilleta, M.; Nguyen, N.-V.; Cleuziou, J.-P.; Klyatskaya, S.; Ruben, M.; Wernsdorfer, W. Molecular Quantum Spintronics: Supramolecular Spin Valves Based on Single-Molecule Magnets and Carbon Nanotubes. *Int. J. Mol. Sci.* **2011**, *12*, 6656–6667. [[CrossRef](#)] [[PubMed](#)]
4. Sanvito, S. Molecular Spintronics. *Chem. Soc. Rev.* **2011**, *40*, 3336. [[CrossRef](#)]
5. Thiele, S.; Vincent, R.; Holzmann, M.; Klyatskaya, S.; Ruben, M.; Balestro, F.; Wernsdorfer, W. Electrical Readout of Individual Nuclear Spin Trajectories in a Single-Molecule Magnet Spin Transistor. *Phys. Rev. Lett.* **2013**, *111*, 037203. [[CrossRef](#)]
6. Gobbi, M.; Novak, M.A.; Del Barco, E. Molecular Spintronics. *J. Appl. Phys.* **2019**, *125*, 240401. [[CrossRef](#)]
7. Mannini, M.; Pineider, F.; Sainctavit, P.; Danieli, C.; Otero, E.; Sciancalepore, C.; Talarico, A.M.; Arrio, M.-A.; Cornia, A.; Gatteschi, D.; et al. Magnetic Memory of a Single-Molecule Quantum Magnet Wired to a Gold Surface. *Nat. Mater.* **2009**, *8*, 194–197. [[CrossRef](#)]
8. Leuenberger, M.N.; Loss, D. Quantum Computing in Molecular Magnets. *Nature* **2001**, *410*, 789–793. [[CrossRef](#)] [[PubMed](#)]
9. Krylov, A.I.; Doyle, J.; Ni, K.-K. Quantum Computing and Quantum Information Storage. *Phys. Chem. Chem. Phys.* **2021**, *23*, 6341–6343. [[CrossRef](#)]
10. Winpenny, R.E.P. Quantum Information Processing Using Molecular Nanomagnets as Qubits. *Angew. Chem. Int. Ed.* **2008**, *47*, 7992–7994. [[CrossRef](#)]
11. Waldmann, O. A Criterion for the Anisotropy Barrier in Single-Molecule Magnets. *Inorg. Chem.* **2007**, *46*, 10035–10037. [[CrossRef](#)] [[PubMed](#)]
12. Neese, F.; Pantazis, D.A. What Is Not Required to Make a Single Molecule Magnet. *Faraday Discuss.* **2011**, *148*, 229–238. [[CrossRef](#)] [[PubMed](#)]
13. Harriman, K.L.M.; Errulat, D.; Murugesu, M. Magnetic Axiality: Design Principles from Molecules to Materials. *Trends Chem.* **2019**, *1*, 425–439. [[CrossRef](#)]
14. Goodwin, C.A.P.; Ortu, F.; Reta, D.; Chilton, N.F.; Mills, D.P. Molecular Magnetic Hysteresis at 60 Kelvin in Dysprosocenium. *Nature* **2017**, *548*, 439–442. [[CrossRef](#)] [[PubMed](#)]
15. Guo, F.-S.; Day, B.M.; Chen, Y.-C.; Tong, M.-L.; Mansikkamäki, A.; Layfield, R.A. Magnetic Hysteresis up to 80 Kelvin in a Dysprosium Metallocene Single-Molecule Magnet. *Science* **2018**, *362*, 1400–1403. [[CrossRef](#)] [[PubMed](#)]
16. Sorace, L.; Gatteschi, D. Electronic Structure and Magnetic Properties of Lanthanide Molecular Complexes. In *Lanthanides and Actinides in Molecular Magnetism*; Wiley-VCH Verlag GmbH & Co. KGaA: Weinheim, Germany, 2015; pp. 1–26.
17. Liddle, S.T.; van Slageren, J. Improving f-Element Single Molecule Magnets. *Chem. Soc. Rev.* **2015**, *44*, 6655–6669. [[CrossRef](#)]
18. Perfetti, M.; Bendix, J. The Multiple Faces, and Phases, of Magnetic Anisotropy. *Inorg. Chem.* **2019**, *58*, 11875–11882. [[CrossRef](#)]
19. Dei, A.; Gatteschi, D.; Pécaut, J.; Poussereau, S.; Sorace, L.; Vostrikova, K. Crystal Field and Exchange Effects in Rare Earth Semiquinone Complexes. *Comptes Rendus L'Académie Sci. Ser. IIC-Chem.* **2001**, *4*, 135–141. [[CrossRef](#)]
20. Demir, S.; Jeon, I.-R.; Long, J.R.; Harris, T.D. Radical Ligand-Containing Single-Molecule Magnets. *Coord. Chem. Rev.* **2015**, *289–290*, 149–176. [[CrossRef](#)]
21. Briganti, M.; Lucaccini, E.; Chelazzi, L.; Ciattini, S.; Sorace, L.; Sessoli, R.; Totti, F.; Perfetti, M. Magnetic Anisotropy Trends along a Full 4f-Series: The  $f^{l+7}$  Effect. *J. Am. Chem. Soc.* **2021**, *143*, 8108–8115. [[CrossRef](#)]
22. Zhu, Z.; Guo, M.; Li, X.-L.; Tang, J. Molecular Magnetism of Lanthanide: Advances and Perspectives. *Coord. Chem. Rev.* **2019**, *378*, 350–364. [[CrossRef](#)]
23. Parmar, V.S.; Mills, D.P.; Winpenny, R.E.P. Mononuclear Dysprosium Alkoxide and Aryloxide Single-Molecule Magnets. *Chem. A Eur. J.* **2021**, *27*, 7625–7645. [[CrossRef](#)]
24. Wang, J.; Li, Q.; Wu, S.; Chen, Y.; Wan, R.; Huang, G.; Liu, Y.; Liu, J.; Reta, D.; Giansiracusa, M.J.; et al. Opening Magnetic Hysteresis by Axial Ferromagnetic Coupling: From Mono-Decker to Double-Decker Metallacrown. *Angew. Chem. Int. Ed.* **2021**, *60*, 5299–5306. [[CrossRef](#)]

25. Canaj, A.B.; Dey, S.; Martí, E.R.; Wilson, C.; Rajaraman, G.; Murrie, M. Insight into D<sub>6h</sub> Symmetry: Targeting Strong Axiality in Stable Dysprosium(III) Hexagonal Bipyramidal Single-Ion Magnets. *Angew. Chem. Int. Ed.* **2019**, *58*, 14146–14151. [[CrossRef](#)] [[PubMed](#)]
26. Sørensen, M.A.; Hansen, U.B.; Perfetti, M.; Pedersen, K.S.; Bartolomé, E.; Simeoni, G.G.; Mutka, H.; Rols, S.; Jeong, M.; Zivkovic, I.; et al. Chemical Tunnel-Splitting-Engineering in a Dysprosium-Based Molecular Nanomagnet. *Nat. Commun.* **2018**, *9*, 1292. [[CrossRef](#)]
27. Perfetti, M.; Caneschi, A.; Sukhikh, T.S.; Vostrikova, K.E. Lanthanide Complexes with a Tripodal Nitroxyl Radical Showing Strong Magnetic Coupling. *Inorg. Chem.* **2020**, *59*, 16591–16598. [[CrossRef](#)]
28. Ito, A.; Nakano, Y.; Urabe, M.; Tanaka, K.; Shiro, M. Structural and Magnetic Studies of Copper(II) and Zinc(II) Coordination Complexes Containing Nitroxide Radicals as Chelating Ligands. *Eur. J. Inorg. Chem.* **2006**, *2006*, 3359–3368. [[CrossRef](#)]
29. Gass, I.A.; Gartshore, C.J.; Lupton, D.W.; Moubaraki, B.; Nafady, A.; Bond, A.M.; Boas, J.F.; Cashion, J.D.; Milsmann, C.; Wieghardt, K.; et al. Anion Dependent Redox Changes in Iron Bis-Terdentate Nitroxide {NNO} Chelates. *Inorg. Chem.* **2011**, *50*, 3052–3064. [[CrossRef](#)] [[PubMed](#)]
30. Gass, I.A.; Tewary, S.; Nafady, A.; Chilton, N.F.; Gartshore, C.J.; Asadi, M.; Lupton, D.W.; Moubaraki, B.; Bond, A.M.; Boas, J.F.; et al. Observation of Ferromagnetic Exchange, Spin Crossover, Reductively Induced Oxidation, and Field-Induced Slow Magnetic Relaxation in Monomeric Cobalt Nitroxides. *Inorg. Chem.* **2013**, *52*, 7557–7572. [[CrossRef](#)]
31. Gass, I.A.; Tewary, S.; Rajaraman, G.; Asadi, M.; Lupton, D.W.; Moubaraki, B.; Chastanet, G.; Létard, J.-F.; Murray, K.S. Solvate-Dependent Spin Crossover and Exchange in Cobalt(II) Oxazolidine Nitroxide Chelates. *Inorg. Chem.* **2014**, *53*, 5055–5066. [[CrossRef](#)]
32. Gass, I.A.; Asadi, M.; Lupton, D.W.; Moubaraki, B.; Bond, A.M.; Guo, S.-X.; Murray, K.S. Manganese(II) Oxazolidine Nitroxide Chelates: Structure, Magnetism, and Redox Properties. *Aust. J. Chem.* **2014**, *67*, 1618. [[CrossRef](#)]
33. Pedersen, A.H.; Geoghegan, B.L.; Nichol, G.S.; Lupton, D.W.; Murray, K.S.; Martínez-Lillo, J.; Gass, I.A.; Brechin, E.K. Hexahalorhenate(IV) Salts of Metal Oxazolidine Nitroxides. *Dalt. Trans.* **2017**, *46*, 5250–5259. [[CrossRef](#)] [[PubMed](#)]
34. Gass, I.A.; Lu, J.; Asadi, M.; Lupton, D.W.; Forsyth, C.M.; Geoghegan, B.L.; Moubaraki, B.; Cashion, J.D.; Martin, L.L.; Bond, A.M.; et al. Use of the TCNQF<sub>4</sub><sup>2-</sup> Dianion in the Spontaneous Redox Formation of [Fe<sup>III</sup>(L<sup>-</sup>)<sub>2</sub>][TCNQF<sub>4</sub><sup>•-</sup>]. *Chempluschem* **2018**, *83*, 658–668. [[CrossRef](#)]
35. Gass, I.A.; Lu, J.; Ojha, R.; Asadi, M.; Lupton, D.W.; Geoghegan, B.L.; Moubaraki, B.; Martin, L.L.; Bond, A.M.; Murray, K.S. [Fe<sup>II</sup>(L<sup>•</sup>)<sub>2</sub>][TCNQF<sub>4</sub><sup>•-</sup>]<sub>2</sub>: A Redox-Active Double Radical Salt. *Aust. J. Chem.* **2019**, *72*, 769–777. [[CrossRef](#)]
36. Liu, B.-C.; Ge, N.; Zhai, Y.-Q.; Zhang, T.; Ding, Y.-S.; Zheng, Y.-Z. An Imido Ligand Significantly Enhances the Effective Energy Barrier of Dysprosium(III) Single-Molecule Magnets. *Chem. Commun.* **2019**, *55*, 9355–9358. [[CrossRef](#)] [[PubMed](#)]
37. Benamara, N.; Diop, M.; Leuvrey, C.; Lenertz, M.; Gilliot, P.; Gallart, M.; Bolvin, H.; Setifi, F.; Rogez, G.; Rabu, P.; et al. Octahedral Hexachloro Environment of Dy<sup>3+</sup> with Slow Magnetic Relaxation and Luminescent Properties. *Eur. J. Inorg. Chem.* **2021**, *2021*, 2099–2107. [[CrossRef](#)]
38. Andrews, P.C.; Beck, T.; Forsyth, C.M.; Fraser, B.H.; Junk, P.C.; Massi, M.; Roesky, P.W. Templated Assembly of a μ<sub>6</sub>-CO<sub>3</sub><sup>2-</sup> Dodecanuclear Lanthanum Dibenzoylemethanide Hydroxido Cluster with Concomitant Formation of Phenylglyoxylate. *Dalt. Trans.* **2007**, 5651–5654. [[CrossRef](#)]
39. Sukhikh, T.S.; Kolybalov, D.S.; Pylova, E.K.; Bashirov, D.A.; Komarov, V.Y.; Kuratieva, N.V.; Smolentsev, A.I.; Fitch, A.N.; Konchenko, S.N. A Fresh Look at the Structural Diversity of Dibenzoylemethanide Complexes of Lanthanides. *New J. Chem.* **2019**, *43*, 9934–9942. [[CrossRef](#)]
40. Johnston, D.H.; Shriver, D.F. Vibrational Study of the Trifluoromethanesulfonate Anion: Unambiguous Assignment of the Asymmetric Stretching Modes. *Inorg. Chem.* **1993**, *32*, 1045–1047. [[CrossRef](#)]
41. Goodwin, C.A.P.; Chilton, N.F.; Vettese, G.F.; Pineda, E.M.; Crowe, I.F.; Ziller, J.W.; Winpenny, R.E.P.; Evans, W.J.; Mills, D.P. Physicochemical Properties of Near-Linear Lanthanide(II) Bis(Silylamide) Complexes (Ln = Sm, Eu, Tm, Yb). *Inorg. Chem.* **2016**, *55*, 10057–10067. [[CrossRef](#)]
42. Llunell, M.; Casanova, D.; Cirera, J.; Alemany, P.; Alvarez, S. *SHAPE, Version 2.1, Program for the Stereochemical Analysis of Molecular Fragments by Means of Continuous Shape Measures and Associated Tools*; Universitat de Barcelona: Barcelona, Spain, 2013.
43. Long, J.; Lyubov, D.M.; Mahrova, T.V.; Lyssenko, K.A.; Korlyukov, A.A.; Fedorov, Y.V.; Chernikova, E.Y.; Guari, Y.; Larionova, J.; Trifonov, A.A. Heteroleptic Lanthanide Complexes Coordinated by Tripodal Tetradentate Ligand: Synthesis, Structure, and Magnetic and Photoluminescent Properties. *Cryst. Growth Des.* **2020**, *20*, 5184–5192. [[CrossRef](#)]
44. Hamada, D.; Fujinami, T.; Yamauchi, S.; Matsumoto, N.; Mochida, N.; Ishida, T.; Sunatsuki, Y.; Tsuchimoto, M.; Coletti, C.; Re, N. Luminescent Dy<sup>III</sup> Single Ion Magnets with Same N<sub>6</sub>O<sub>3</sub> Donor Atoms but Different Donor Atom Arrangements, 'fac'-[Dy<sup>III</sup>(HL<sup>DL-Ala</sup>)<sub>3</sub>].8H<sub>2</sub>O and 'mer'-[Dy<sup>III</sup>(HL<sup>DL-Phe</sup>)<sub>3</sub>].7H<sub>2</sub>O. *Polyhedron* **2016**, *109*, 120–128. [[CrossRef](#)]
45. Murakami, R.; Nakamura, T.; Ishida, T. Doubly TEMPO-Coordinated Gadolinium(III), Lanthanum(III), and Yttrium(III) Complexes. Strong Superexchange Coupling across Rare Earth Ions. *Dalt. Trans.* **2014**, *43*, 5893–5898. [[CrossRef](#)]
46. Petrochenkova, N.V.; Tkachenko, I.A.; Mirochnik, A.G.; Karasev, V.E.; Kavun, V.Y. Luminescence and Magnetic Properties of Europium(III) Carboxylatodibenzoylemethanates. *Opt. Spectrosc.* **2010**, *109*, 917–920. [[CrossRef](#)]
47. Kahn, M.L.; Sutter, J.-P.; Golhen, S.; Guionneau, P.; Ouahab, L.; Kahn, O.; Chasseau, D. Systematic Investigation of the Nature of the Coupling between a Ln(III) Ion (Ln = Ce(III) to Dy(III)) and Its Aminoxyl Radical Ligands. Structural and Magnetic

- Characteristics of a Series of  $\{\text{Ln}(\text{Radical})_2\}$  Compounds and the Related  $\{\text{Ln}(\text{Nitron})_2\}$  Derivat. *J. Am. Chem. Soc.* **2000**, *122*, 3413–3421. [[CrossRef](#)]
48. Bain, G.A.; Berry, J.F. Diamagnetic Corrections and Pascal's Constants. *J. Chem. Educ.* **2008**, *85*, 532. [[CrossRef](#)]
49. Sheldrick, G.M. SHELXT—Integrated Space-Group and Crystal-Structure Determination. *Acta Crystallogr. Sect. A Found. Adv.* **2015**, *71*, 3–8. [[CrossRef](#)]
50. Sheldrick, G.M. Crystal Structure Refinement with SHELXL. *Acta Crystallogr. Sect. C Struct. Chem.* **2015**, *71*, 3–8. [[CrossRef](#)] [[PubMed](#)]
51. Dolomanov, O.V.; Bourhis, L.J.; Gildea, R.J.; Howard, J.A.K.; Puschmann, H. OLEX2: A Complete Structure Solution, Refinement and Analysis Program. *J. Appl. Crystallogr.* **2009**, *42*, 339–341. [[CrossRef](#)]